IET Generation, Transmission & Distribution

Research Article

IET Journals
The Institution of Engineering and Technology

Local measurement-based technique for estimating fault location in multi-source DC microgrids

ISSN 1751-8687
Received on 18th November 2017
Revised 27th March 2018
Accepted on 24th April 2018
E-First on 22nd May 2018
doi: 10.1049/iet-gtd.2017.1801
www.ietdl.org

Anju Meghwani[1] ✉, *Suresh C. Srivastava*[1], *Saikat Chakrabarti*[1]

[1]*Department of Electrical Engineering, IIT Kanpur, Kanpur, Uttar Pradesh, India*

✉ *E-mail: anjum@iitk.ac.in*

Abstract: Quick fault detection and isolation of faulty section are desired in DC microgrid due to the presence of power electronic converters and low cable impedances. Owing to need of fast disconnection, limited time and data are available for online fault distance estimation. Some of the existing techniques consider source capacitors connected at only one end of the cable; therefore, assume that the fault current is contributed by only one end of the cable. This may not be true in the case of multi-source DC microgrids, where fault current would be supplied from both the ends. Further, existing communication-based techniques require either data synchronisation or fast communication network. To address these issues, this study proposes an online fault location method for multi-source DC microgrid without using communication. The mathematical model of faulted cable section connected to sources at both the ends is derived. This model is used along with the measurements to determine the fault distance. The model consistency with the measurements is quantified using the confidence level based on the residual analysis. A ring-type multi-source DC microgrid system is considered and simulated on real-time digital simulator to demonstrate the effectiveness of the proposed algorithm.

1 Introduction

In recent past, significant research and development efforts have been made to integrate renewable energy sources, such as wind turbines and photovoltaic (PV) systems into the power distribution networks [1, 2]. Along with this, the development in the power electronics had led to the easy integration of the renewable sources with DC microgrids. Key advantage of a DC microgrid when compared with an AC microgrid is that the loads, sources, and energy storage elements can be connected through simpler and more efficient power electronic interfaces [3]. Other advantages include its higher efficiency, ease of paralleling of sources on the DC bus, and more power transfer capacity [4–6]. Nonetheless, the realisation of the DC microgrids is still facing many protection challenges due to the nature of the DC faults [7].

Generally, cables are used in DC microgrid, which offer low interconnecting inductive reactance. As a result, the rate of rise of current is large during the fault. Further, most of the loads and sources in DC microgrid are connected using power electronic converters. Owing to the presence of the output capacitors of the converters, the short-circuit fault current may reach nine to ten times the rated current in short duration [8]. In the case of some converters (such as DC–DC boost, dual active bridge etc.), after the capacitor discharges below a critical value, the high fault current finds its path through the power semiconductor devices of the converters. These converters are not designed to allow such large currents due to the electrical and other physical limits of the power semiconductor devices. Therefore, fast detection and disconnection of fault is required so as to protect these converters.

A fast current differential protection scheme is suggested in [9]. In this scheme, a high bandwidth communication channel is required to transmit analogue current signal. Other protection schemes utilising low bandwidth communication network are suggested in [10–12]. In these schemes, the fault is identified using di/dt [10, 11], and estimated cable parameters [12] and only decision is transmitted to the other end of the cable to issue the trip signal. Few local measurements-based methods are also discussed in the literature [13, 14]. Technique based on first- and second-order derivative of fault current is suggested in [14]. In another scheme, a parallel LC tank circuit is deployed in series with relay to generate the oscillation at resonant frequency during the fault. The identification of frequency in the line current generates the trip signal for the protection devices. The aforementioned methods have discussed the fast detection of the fault and followed by disconnection of faulty section. However, the location of the fault is not determined in these methods.

Automatic fault location in microgrids is important for its timely maintenance and restoration, specifically in critical applications such as ship, space station, military base, and islands. It is also required for network with underground cables, where visual inspection is not viable [15, 16]. Fast determination of the fault location helps in early restoration, thereby increasing the resiliency of the microgrid [17, 18]. Generally, fast fault detection methods are used for quick isolation and then offline methods are utilised for determination of fault location. Voltage or current signal is injected into the faulty cable using an external circuit. The resultant signals due to the injection are measured and analysed to determine the location of the fault. Few methods based on injecting a DC signal employing a charged capacitor circuit known as power probe unit (PPU) are discussed in [19–21]. Few power electronics converter-based PPUs for injecting AC signals are suggested in [22–25]. In spite of the fact that these methods operate well, an additional equipment such as PPU is required to be connected to each cable section. It may increase the overall cost of the system. Even for the portable PPUs, human intervention is required, thereby adding to the cost. Therefore, online methods for determination of fault location are discussed in the literature, which does not require additional signal injection, thereby reducing the cost. These methods use voltage and current measurements during the fault, to estimate its location. However, as fast location and isolation of fault is desirable in DC microgrid, less time period/data is available for estimation of the fault distance.

Techniques for online estimation of fault location in DC systems are reported in [26–29]. These methods utilise travelling wave-based phenomenon to determine the location of fault. However, these methods may not give accurate results in the case of DC microgrids with small cable lengths, due to small surge arrival time. Recently, a differential current measurement-based fault location technique is discussed in [30]. In this work, the fault is located by considering the current measurements from both the ends of the faulty cable. Ethernet is suggested for communicating parameter values from one end of the cable to other end. Data is

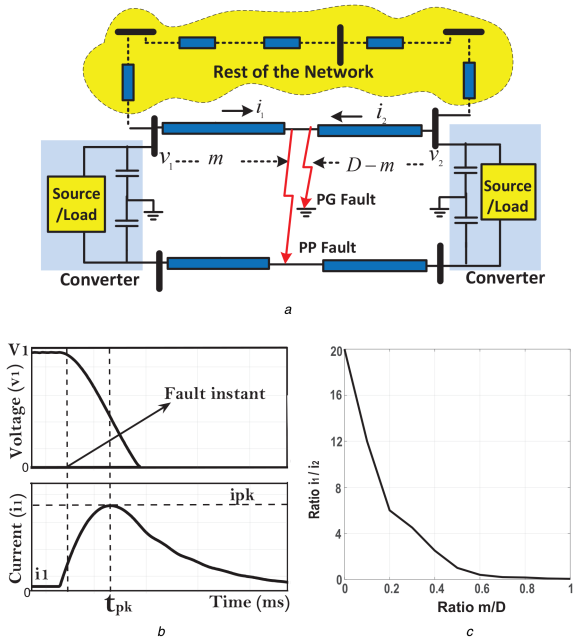

Fig. 1 *DC microgrid faulted network section and its transients*
(a) Faulted network section, ***(b)*** Representative waveforms of line current i_1 and DC bus voltage v_1 during fault, ***(c)*** Ratio of currents contributed from both ends of cable (i_1/i_2)

not synchronised due to small distances in the DC system and use of fast communication (Ethernet) media. Techniques based on local measurements, without using communication, for online fault location are suggested in [7, 31]. In [7], the voltage and current measurements, captured at various time instances, are substituted in their respective mathematical equation to estimate the fault distance. Another method suggested in [31] estimates the fault location by utilising the local voltage, current, and current derivative. The models used in both the aforementioned methods [7, 31] are based on the DC network in which capacitor is connected at only one end of the cable. Therefore, it is assumed that the fault current would be only supplied from one end of the cable. This may not be the case in DC microgrids, where various power electronic loads and sources are connected at both the ends of the cable. These power electronic devices have capacitors on the microgrid side, which contribute to the fault currents from both the ends of the cable.

To address the aforementioned issues, this paper proposes an online fault location scheme, which does not require communication. The scheme is generic and considers sources and loads connected at both ends of the cables. A suitable mathematical model of the faulty cable is determined considering capacitance connected at both ends of the cable. The model is used along with local measurements to determine the location of the fault. To quantify the consistency of the model with the measurements, a confidence level is defined based on the residual analysis.

The remaining paper is organised as follows. In Section 2, the challenges and requirements of online fault location technique in DC microgrid are discussed. The proposed method is discussed in Section 3. Modelling of the faulty cable with capacitors at both ends is also included. The proposed algorithm is validated on a DC microgrid using the numerical simulation on real-time digital simulator (RTDS). The results are presented in Section 4. Finally, the main conclusions are provided in Section 5.

2 Challenges in online fault location

An online fault location algorithm should be fast, robust, reliable, and capable of locating the fault with high accuracy. The two basic requirements are to locate the fault within allowed time interval, and the designed algorithm should be independent of the grid architecture. Before explaining the proposed fault location technique, these two requirements are discussed in the following sections.

2.1 Available execution time

A typical DC microgrid consists of power electronic converters to interface various sources and loads, as shown in Fig. 1*a*. These converters have capacitors connected on the DC microgrid side, to absorb the high-frequency ripple current. These capacitors contribute large currents to the fault transients. Further, low impedance offered by the cable is unable to limit the high rate of rise of the fault current. As a result, the line current (i_1) increases, reaching to its peak value at t_{pk}, as shown in Fig. 1*b*.

These types of faults are required to be detected much before the current reaches its peak value t_{pk}. Theoretically, the allowed time t_{fl} to detect the fault is given by

$$t_{fl} = t_{cr} - t_{cb} - t_{misc} \tag{1}$$

where t_{cb} is the breaker operating time, and it is normally 500 µs for hybrid and solid-state CB [32, 33]. Time t_{cr} is the critical time [34]. Other miscellaneous delays t_{misc} include the communication delay associated with the data transfer, processing delays etc. Owing to small value of t_{fl} in DC microgrid, less number of measured data is available for estimation of location using fault transients. The aim of this work is to develop fault location algorithm, which can estimate the fault location before the isolation of the faulty section.

2.2 Microgrid architecture

In a conventional distribution system, the power sources are connected upstream and loads are connected downstream. In such systems, fault current is supplied by the upstream bus. However, in DC microgrid architecture, multiple power electronic converters interfacing sources and loads are distributed in the system. In this case, the fault current is supplied from both ends of the cable, unlike the conventional system. Plot of the ratio of the currents supplied from the two ends of the cable with fault distance (m) is shown in Fig. 1*c*. It is observed that the currents contributed from both the ends are almost equal for fault in the middle of the cable. Further, it is noticed that the contribution of the current reduces as the fault moves away from the corresponding bus. Since the current is contributed from both ends of the cable, the data monitoring may be required at both ends to determine the accurate location of the fault. To process the data, synchronisation of the data may be required using global positioning system or fast communication may be utilised with small delays. However, using communication increases cost. Further, it may reduce reliability in the case of communication link failure along with power cable fault.

In summary, a scheme for fast fault location estimation using fault transients is required in DC microgrids. Large penetration of power electronic converters increases the challenges by allowing fault current to flow from both ends of the cable. Using communication may increase cost and reduce the reliability of fault location technique.

3 Proposed fault location technique

To develop the fault location algorithm, first the analytical model of the faulted zone of the network is derived. The model is developed with reference to Fig. 2, which shows the fault location m and capacitors connected at both ends of the cable. The derived model, accompanied by the local measurements, is used to determine the fault distance and its resistance.

3.1 Faulted zone model

The state space equation, for the faulted network with pole-to-pole fault, as shown in Fig. 2*a* is written as

$$v_1 = l_1\frac{\mathrm{d}i_1}{\mathrm{d}t} + r_1 i_1 + i_2(r_1 + R_f) \tag{2a}$$

$$v_2 = (L_c - l_1)\frac{\mathrm{d}i_2}{\mathrm{d}t} + (R_c - r_1)i_2 + i_1(R_c - r_1 + R_f) \tag{2b}$$

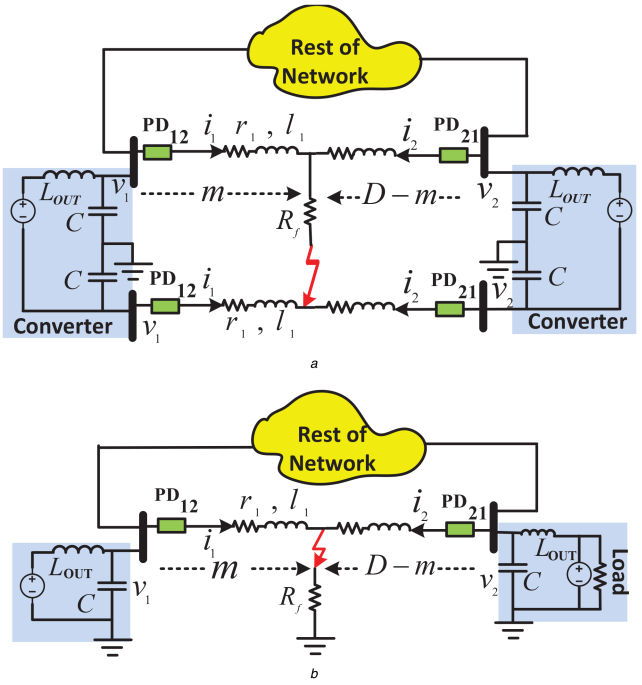

Fig. 2 *Equivalent faulted network*
(a) Pole-to-pole (PP) fault, ***(b)*** Pole-to-ground (PG) fault

where l_1, r_1 represent the equivalent cable inductance and resistance up to the fault point, respectively, and R_f is the fault resistance. L_c and R_c are the cable parameters for 100% cable length. Voltages, v_1, v_2, are the pole–pole voltage at buses 1 and 2, respectively. Currents, i_1, i_2, are the line currents observed at the two ends of the cable during fault. In the case of pole-to-ground fault (shown in Fig. 2*b*), (2) is applicable by replacing l_1, r_1, and L, R with equivalent inductance and resistance of pole–ground circuit and replacing voltages v_1, v_2 by the pole to ground voltages. In the case of pole–pole fault (Fig. 2*a*), the cable parameters in terms of the fault distance m are written as

$$r_1 = mR, \quad l_1 = mL, \quad R_c = DR, \quad L_c = DL \tag{3}$$

where m is the cable length from PD_{12} up to the fault point in km, L, R are the inductance and resistance per unit length of the cable, and D is the total length of the cable. Subtracting (2b) from (2a), and substituting r_1, l_1, R_c, and L_c from (3) gives

$$v_1 - v_2 - mL\frac{\mathrm{d}i_1}{\mathrm{d}t} - mRi_1 + (D-m)L\frac{\mathrm{d}i_2}{\mathrm{d}t} + (D-m)Ri_2 = 0 \tag{4}$$

As the fault occurs, the capacitors, connected at both ends, discharge and contribute to the fault current. The fault currents contributed by the capacitors at buses 1 and 2 (ends of the cable) are larger when compared with the rest of the network. This is due to the presence of the interconnecting cables between the sources connected in rest of the network. Current i_2 during the fault transient is related to v_2 as

$$v_2 = -\frac{1}{C}\int i_2\,\mathrm{d}t \tag{5}$$

Substituting v_2 from (5) in (4) gives

$$v_1 + \frac{1}{C}\int i_2\,\mathrm{d}t - mL\frac{\mathrm{d}i_1}{\mathrm{d}t} - \mathrm{d}Ri_1 + (D-m)L\frac{\mathrm{d}i_2}{\mathrm{d}t} + (D-m)Ri_2 = 0 \tag{6}$$

Substituting i_2 from (2a) in (6) and rearranging gives

$$H_1m^2 + H_2m + H_3R_f + I = Y \tag{7}$$

where I is an integration constant (depends on initial conditions) and H_1, H_2, H_3, and Y are coefficients, given as

$$H_1 = R^2Ci_1 + 2RLC\frac{\mathrm{d}i_1}{\mathrm{d}t} + L^2C\frac{\mathrm{d}^2i_1}{\mathrm{d}t^2} \tag{8}$$

$$H_2 = -RCv_1 - Li_1 - R^2CDi_1 - 2DRLC\frac{\mathrm{d}i_1}{\mathrm{d}t} - R\int i_i\,\mathrm{d}t - LC\frac{\mathrm{d}v_1}{\mathrm{d}t} - L^2DC\frac{\mathrm{d}^2i_1}{\mathrm{d}t^2} \tag{9}$$

$$H_3 = v_1C - LC\frac{\mathrm{d}i_1}{\mathrm{d}t} - RCi_1 - \int i_1\,\mathrm{d}t \tag{10}$$

$$Y = -DRCv_1 - \int v_1\,\mathrm{d}t - DLC\frac{\mathrm{d}v_1}{\mathrm{d}t} \tag{11}$$

Differentiating (7) gives

$$\dot{Y} = m^2\dot{H}_1 + \dot{H}_2m + \dot{H}_3R_\mathrm{f} \tag{12}$$

Equation (12) is used in the proposed method to determine the values of cable fault distance m and fault resistance R_f, as discussed in the following subsection.

3.2 Fault distance and resistance estimation

Coefficients $\dot{H}_1$ to $\dot{H}_3$ and $\dot{Y}$ are calculated at each time interval by assuming the sampling time of Δt. Equation (12) for different time instances in matrix form is written as

$$\begin{bmatrix} \dot{Y}(t) \\ \dot{Y}(t+\Delta t) \\ . \\ . \\ \dot{Y}(t+N\Delta t) \end{bmatrix} = \begin{bmatrix} m^2 & m & R_\mathrm{f} \end{bmatrix} \begin{bmatrix} \dot{H}_1(t) & \dot{H}_2(t) & \dot{H}_3(t) \\ \dot{H}_1(t+\Delta t) & \dot{H}_2(t+\Delta t) & \dot{H}_3(t+\Delta t) \\ . & . & . \\ . & . & . \\ \dot{H}_1(t+N\Delta t) & \dot{H}_2(t+N\Delta t) & \dot{H}_3(t+N\Delta t) \end{bmatrix}^\mathrm{T} \tag{13}$$

where N is the number of samples available for analysis. The above equation in the compact format is written as

$$\boldsymbol{y} = \boldsymbol{H}\boldsymbol{x}^\mathrm{T} \tag{14}$$

To convert the quadratic polynomial function into linear form, (13) is partially differentiated with respect to m and R_f, which provides

$$\begin{bmatrix} \Delta\dot{Y}(t) \\ \Delta\dot{Y}(t+\Delta t) \\ . \\ . \\ \Delta\dot{Y}(t+N\Delta t) \end{bmatrix} = \begin{bmatrix} \frac{\partial\dot{Y}(t)}{\partial m} & \frac{\partial\dot{Y}(t)}{\partial R_\mathrm{f}} \\ \frac{\partial\dot{Y}(t+\Delta t)}{\partial m} & \frac{\partial\dot{Y}(t+\Delta t)}{\partial R_\mathrm{f}} \\ . & \\ . & \\ \frac{\partial\dot{Y}(t+N\Delta t)}{\partial m} & \frac{\partial\dot{Y}(t+N\Delta t)}{\partial R_\mathrm{f}} \end{bmatrix} \cdot \begin{bmatrix} \Delta m \\ \Delta R_\mathrm{f} \end{bmatrix} \tag{15}$$

This set of equations is written into matrix form as

$$\Delta\boldsymbol{y} = \boldsymbol{H}_d\Delta\boldsymbol{x} \tag{16}$$

where Jacobian matrix $\boldsymbol{H}_d$ is

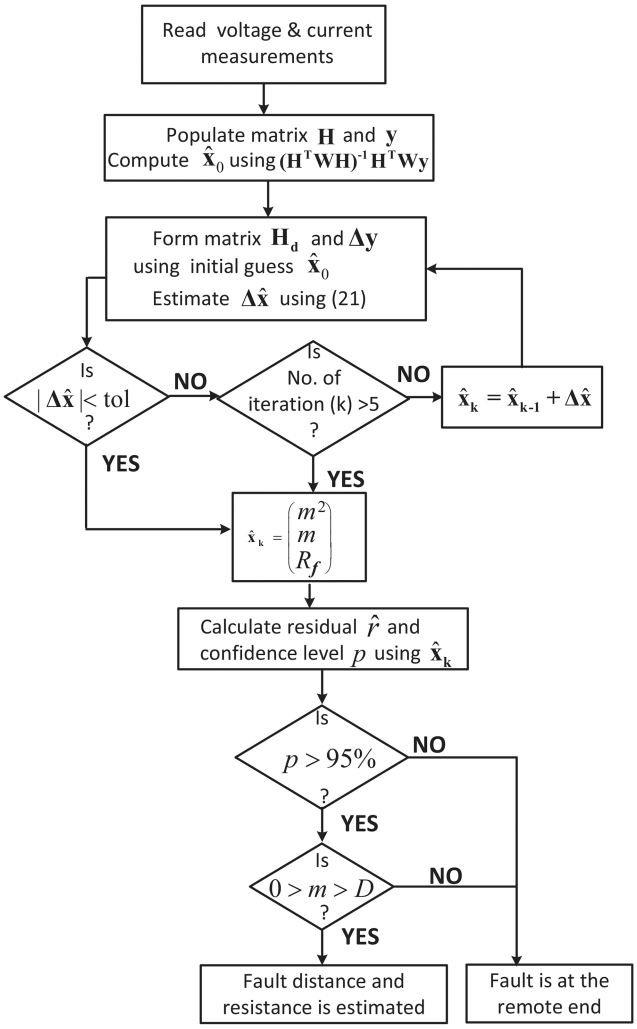

Fig. 3 *Flowchart of the proposed fault location algorithm*

$$\boldsymbol{H}_d = \begin{bmatrix} 2m\dot{H}_1(t) + \dot{H}_2(t) & \dot{H}_3(t) \\ 2m\dot{H}_1(t+\Delta t) + \dot{H}_2(t+\Delta t) & \dot{H}_3(t+\Delta t) \\ . & . \\ . & . \\ 2m\dot{H}_1(t+N\Delta t) + \dot{H}_2(t+N\Delta t) & \dot{H}_3(t+N\Delta t) \end{bmatrix} \tag{17}$$

Factors $\dot{H}_1$–$\dot{H}_3$ are function of time. Further, $\epsilon_{\boldsymbol{y}}$ is defined as the error between the actual measurement and the estimated measurement vector $\boldsymbol{H}_d\Delta\hat{\boldsymbol{x}}$

$$\epsilon_{\boldsymbol{y}} = \Delta\boldsymbol{y} - \boldsymbol{H}_d\Delta\hat{\boldsymbol{x}} \tag{18}$$

where $\Delta\hat{\boldsymbol{x}}$ is the estimated change in the cable parameters from their initial guess value. Traditional state estimator is formulated as the least square optimisation problem by minimising the function

$$\boldsymbol{O} = \epsilon_{\boldsymbol{y}}^{\mathrm{T}}\boldsymbol{W}\epsilon_{\boldsymbol{y}} \tag{19}$$

where $\boldsymbol{W}$ is the weight assigned to the measurements, given as

$$\boldsymbol{W} = \mathrm{diag}\left\{1/\sigma_1^2, 1/\sigma_i^2, \ldots, 1/\sigma_N^2\right\} \tag{20}$$

The σ_i is the standard deviation of the error in measurement. Using (18)–(20), $\boldsymbol{O}$ is minimised, and the solution $\boldsymbol{\Delta\hat{x}}$ is written as

$$\Delta\hat{\boldsymbol{x}} = (\boldsymbol{H}_d^{\mathrm{T}}\boldsymbol{W}\boldsymbol{H}_d)^{-1}\boldsymbol{H}_d^{\mathrm{T}}\boldsymbol{W}\Delta\boldsymbol{y} \tag{21}$$

The above derived expressions are utilised to develop the fault location algorithm. The major steps of the proposed algorithm are given in the following section.

3.3 Proposed algorithm

The proposed fault location algorithm requires locally sampled voltage and current measurements. The computational steps of the algorithm are:

1. Populate matrix $\boldsymbol{H}$ and $\boldsymbol{y}$ of (14) using (13) for window length of N samples. Compute the initial estimated values of the fault distance m and the resistance R_{f} using $\hat{\boldsymbol{x}}_{\boldsymbol{0}} = (\boldsymbol{H}^{\mathrm{T}}\boldsymbol{W}\boldsymbol{H})^{-1}\boldsymbol{H}^{\mathrm{T}}\boldsymbol{W}\boldsymbol{y}$.
2. Compute matrix $\boldsymbol{H}_d$ using $\hat{\boldsymbol{x}}_{\boldsymbol{0}}$ and assemble matrix $\Delta\boldsymbol{y}$ using (15)–(17) for N consecutive samples.
3. Solve for $\Delta\hat{\boldsymbol{x}}_k$ using (21), and $\hat{\boldsymbol{x}}_k$ is written as

$$\hat{\boldsymbol{x}}_k = \hat{\boldsymbol{x}}_{k-1} + \begin{bmatrix} \Delta\hat{x}_1^2 \\ \Delta\hat{x}_1 \\ \Delta\hat{x}_2 \end{bmatrix}_k \tag{22}$$

   where $\hat{\boldsymbol{x}}_k$ is the estimated cable parameters at the kth iteration and $\Delta\hat{x}_1, \Delta\hat{x}_2$ are the first and the second element of $\Delta\hat{\boldsymbol{x}}$, i.e. fault distance m and resistance R_{f}.
4. Repeat steps 2–3 till $\Delta\hat{\boldsymbol{x}}$ becomes less than pre-specified tolerance value.
5. Calculate the residual, or the difference between the actual $\boldsymbol{Hx}$ and the estimated $\boldsymbol{H}\hat{\boldsymbol{x}}$ as:

$$\hat{\boldsymbol{r}} = \boldsymbol{y} - \boldsymbol{H}\hat{\boldsymbol{x}} \tag{23}$$

6. If the measurements match with the derived model, i.e. residuals are less than the threshold χ_{th}, it implies that the fault is in its zone of protection. If these are much larger than the metering error, it implies that the disturbance is out of modelled network zone. To quantify the analysis, the residual vector $\boldsymbol{\zeta}$ and the confidence level p are defined as

$$\boldsymbol{\zeta} = \hat{\boldsymbol{r}}^{\mathrm{T}} \cdot \hat{\boldsymbol{r}} \tag{24}$$

$$p = P(\chi^2 \geq \boldsymbol{\zeta}) = 1 - P(\boldsymbol{\zeta}, v) \tag{25}$$

   where $P(\boldsymbol{\zeta}, v)$ is the probability of χ^2 distribution with $\chi^2 \leq \boldsymbol{\zeta}$, and v degree of freedom. This process is based on the χ^2 test [35]. A high confidence level, >95%, describes a good consistency between the measurements and the circuit model. The low confidence level implies that the fault is in adjacent cable.
7. The fault is within its zone if the estimated distance m is positive and less than the total cable length D.

The proposed fault location technique is implemented with a moving window. The overall flowchart of the technique is shown in Fig. 3.

4 Numerical simulation

Numerical simulations have been carried out to validate the proposed technique to estimate the fault distance. In this section, DC microgrid architecture and its components rating are discussed in brief. Various fault scenarios are created to demonstrate the accuracy of fault location algorithm.

4.1 Test system

A low voltage ±0.6 kV bipolar DC microgrid system, as shown in Fig. 4, has been simulated in RTDS. The converter transients are obtained with a small time step of 5 μs and the controller with large time step of 100 μs. The voltage and current measurements are sampled at 20 kHz. Two-level converters are considered to interface DC grid with the renewable sources and AC grid, whereas

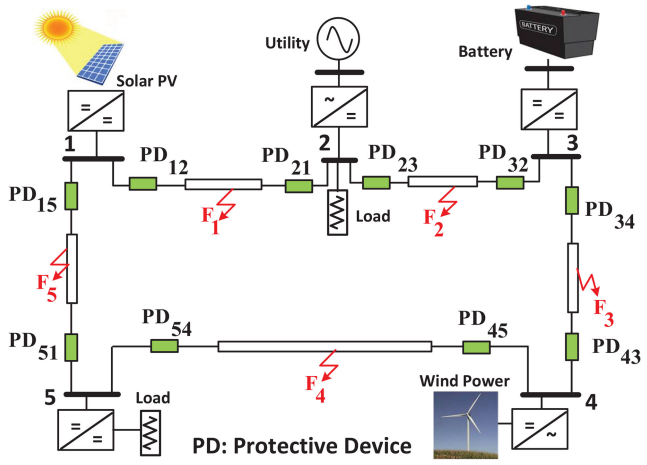

Fig. 4 *Single-line diagram of ring type DC microgrid test system*

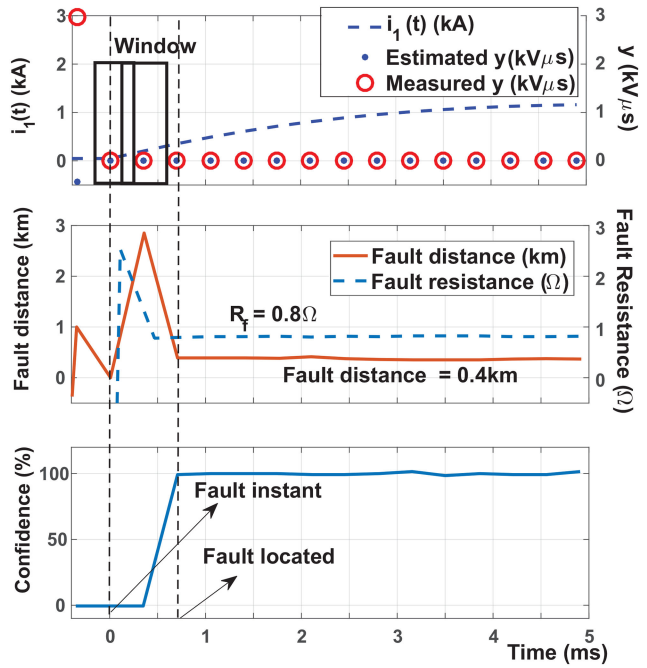

Fig. 5 *Plot of line current, estimated and measured quantities, and estimated fault distance and resistance with confidence level for pole-to-ground fault*

DC/DC converters are used to integrate the battery storage and solar PV system. Component ratings of all the modules are given in Table 1.

A TN-S grounding scheme is employed in the microgrid shown in Fig. 4, where the midpoint of the DC-link is grounded [37]. In this system, the positive and negative poles are at equal potential difference with respect to the ground. From protection design point of view, the grid is equipped with the protective devices (PDs), each placed on positive and negative pole and on both the sides of the DC cable. PD consists of the voltage and the current measuring devices along with the digital relay to process the sampled data. The current direction of all the PDs is assumed as positive towards the cable. The measurement errors are considered as, ±1 and ±2% in the voltage and the current, respectively [38, 39].

4.2 Cable fault with single source and load

A DC network, where sources and loads are connected at both ends of a single cable, is considered to test the algorithm. The cable length is assumed to be 1 km. The two unknowns (m, R_f) are estimated in this system. The algorithm is implemented with a overlapping moving window, as shown in Fig. 5, where a window consists of sets of ten measurements ($N = 10$). Therefore, the degree of freedom (v) for the approximate χ^2 distribution of the objective function $\boldsymbol{O}$ is $N - 2 = 8$. The window is sliding by five measurements until the time t_{fl} is reached. The algorithm is verified for different fault events in the following sections.

Table 1 Rating of DC microgrid components [36]

System component	Rating
DC grid voltage	±0.6 kV
base power	500 kW
battery converter	100 kW
battery	300 V, 1.3 kAh, Nickel Cadmium
PV converter	100 kW
solar panel	$V_{mp} = 54.7$ V, $I_{mp} = 5.58$ A
grid VSC	150 kW
wind turbine	150 kW, PMSG
DC capacitor, C	20 mF
load	constant impedance load 100 kW
cable parameters	
cable cross-section	1000 mm^2 single-core XLPE [13]
cable parameters	$R = 30$ mΩ/km
	$L = 0.97$ mH/km

4.2.1 Fault location under pole-to-ground fault: A fault is considered at 400 m from the PD. A fault resistance R_f of 0.8 Ω is considered in the present case. It is observed that the confidence level before the fault occurrence is <10%, as shown in Fig. 5. At $t = 0.75$ ms, the confidence level becomes >95%. This is because totally ten number of data samples after the fault occurrence are required to locate the fault with high level of confidence. At time $t = 0$, i.e. at the instant of fault inception, the pre-fault data constituting the window are not updated. The fault is accurately located in the third data window. The estimated fault resistance is 0.801 Ω and distance m is 401 m.

4.2.2 Fault location under pole-to-pole fault: A pole-to-pole fault at a distance of 450 m from PD with resistance of 100 mΩ is simulated for the same network. The distance is independently estimated by the two PDs mounted on the positive and the negative poles of the grid. PD at the pole monitors the conductor voltage and current. Positive and negative, as shown in Fig. 6, pole PDs have estimated the distance with 0.22 and 0.23% error, respectively. However, the fault resistances estimated by the positive and negative pole are 50.5 and 51.5 mΩ, respectively. The large error in resistance estimation is due to the fact that during the fault, the resistance seen by each PD becomes half of that of the actual fault resistance, as shown in Fig. 7. Therefore, the actual estimated fault resistance is the sum of the resistance determined by two devices.

4.3 Validation on DC microgrid

The faults in various sections of the DC microgrid, as shown in Fig. 4, are simulated to validate the algorithm for different faulted zones. The algorithm should be able to identify the fault in its zone and should not act for the external faults.

4.3.1 Internal faults: A fault F_1, as shown in Fig. 4, is simulated for different distances and fault resistances. The relative error in the fault distance estimated by the PD at one end of the cable, i.e. PD_{12}, is given in Table 2. It is noticed that the accuracy in estimating the distance reduces as the fault resistance increases, but remains under the limit of 2%. It is due to the fact that the effect of the cable inductance reduces as the fault resistance increases. The contribution of the fault current from the other end dominates as the fault moves closer to it. The effect of other sources present in the DC microgrid is considered by measuring the voltage and current at one end of the cable. Owing to this reason, as the fault moves away, the relative error in the distance estimation increases and becomes >2%, as shown in Table 2. Since the algorithm is implemented in all the PDs, connected at both ends of the cables,

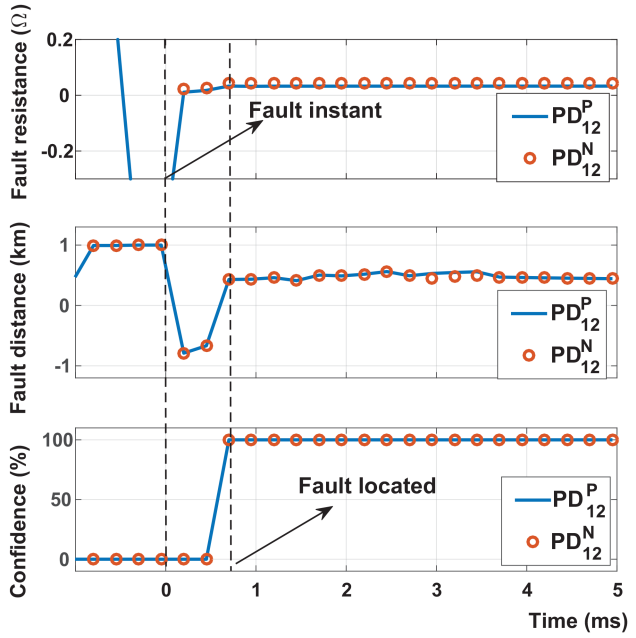

Fig. 6 *Estimated fault resistance and distance along with the confidence level by PDs connected at positive and negative pole for pole-to-pole fault*

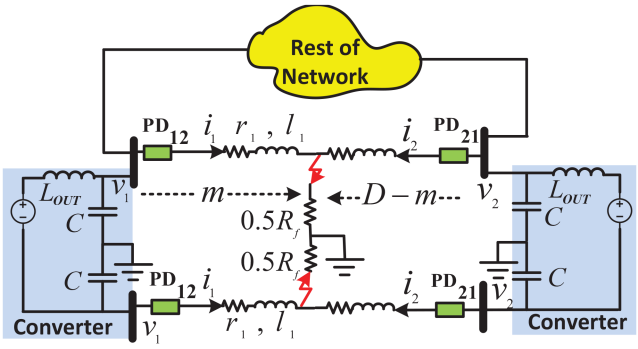

Fig. 7 *Equivalent faulted network for pole-to-pole fault*

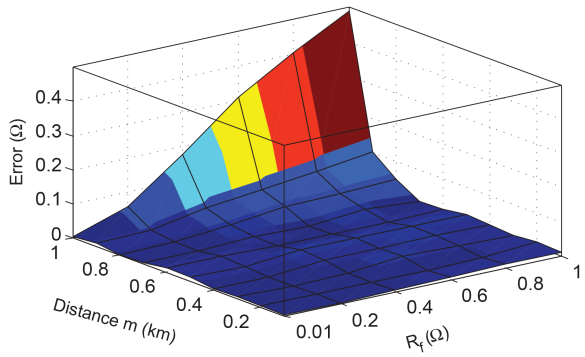

Fig. 8 *Absolute error in estimated resistance for fault F_1 by PD_{12}*

as a result, the fault distance is accurately calculated with the 95% confidence level by at least one of the PDs. The distance is calculated with <2% error for the faults up to 50% of the cable length, as shown in Table 2. In the case of length >50% from PD_{12}, fault is accurately located by PD_{21}, as shown in Table 3.

Similar trend is observed in the fault resistance estimation. PD estimates the fault resistance (R_f) accurately for the faults closer to it, as shown in Fig. 8. The errors in estimating the fault location are almost within 2%.

The execution time of the algorithm is measured for faults at various distance and resistances, as given in Table 4. It is observed that the maximum time taken by the algorithm is <0.25 ms. As the fault moves away from PD_{12}, the execution time of the algorithm increases. This is due to the fact that increase in line inductance

Table 2 Relative error (%) in fault distance estimation by PD_{12}

Fault distance from PD_{12}, km	Resistance R_f, Ω					
	0.01	0.20	0.40	0.60	0.80	1.00
	Error in fault location (ε) in %					
0.05	0.06	0.02	0.04	0.06	0.14	2.00
0.1	0.19	0.20	0.70	1.00	1.00	1.50
0.2	0.24	0.50	0.03	0.50	1.00	2.00
0.3	0.41	0.33	1.00	0.67	1.67	1.67
0.4	0.25	0.75	0.50	0.75	1.25	1.25
0.5	0.60	0.40	0.40	1.20	1.00	0.60
0.6	0.17	0.83	0.57	**8.33**	**8.33**	**8.33**
0.7	0.29	0.43	**7.1**	**8.6**	**6.50**	**3.29**
0.8	0.13	0.25	**6.3**	**3.53**	1.94	**4.6**
0.95	0.32	0.11	**2.8**	**4.5**	1.60	**2.30**

Table 3 Relative error (%) in fault distance estimation by PD_{21}

Fault distance from PD_{21}, km	Resistance R_f, Ω					
	0.01	0.20	0.40	0.60	0.80	1.00
	Error in fault location (ε) in %					
0.05	0.50	0.35	0.41	1.05	1.20	0.67
0.20	0.30	0.87	0.32	0.75	1.25	0.35
0.30	0.41	0.30	0.70	0.67	1.67	1.80
0.40	0.45	0.10	0.50	0.80	2.00	1.50
0.50	0.06	0.35	0.04	0.14	0.06	2.00
0.60	0.15	0.83	0.10	1.05	**12.00**	**5.90**
0.70	0.30	0.87	**7.20**	**8.30**	1.25	0.35
0.80	0.41	1.30	**6.30**	**6.50**	**6.80**	**6.80**
0.90	0.45	10.50	**8.90**	0.80	**12.30**	1.50
0.95	0.85	0.85	**10.50**	**9.80**	**0.06**	**10.10**

results in low rate of rise of current. As a result, the parameters of matrix $\boldsymbol{H}_d$, which depend upon first, second, and third order of current derivative, approach zero. Consequently, the determinant of matrix $\boldsymbol{H}_d$ becomes close to zero and the iteration takes more time due to numerical ill condition.

To further support the numerical simulation, a pole-to-ground fault F_3, as shown in Fig. 4, is simulated. Fault with resistance R_f of 0.8 Ω and at a distance of 0.45 km from PD_{34} is considered. The voltage and current waveforms captured by PDs connected at both ends of the cable, i.e. PD_{34} and PD_{43}, are shown in Fig. 9. It is observed that the presence of fault resistance reduces the rate of rise of current. As a result, pole-to-ground voltage drops to only 595 V.

Another pole-to-pole fault F_3 with low impedance of 20 mΩ and at a distance of 0.25 km from PD_{34} is simulated. Owing to the presence of low fault resistance, the line current rises quickly, as shown in Fig. 10. The proposed algorithm is capable of estimating the fault distance before the pole voltage becomes less than the source voltage.

4.3.2 External faults: The derived model of the faulted network is valid for faults internal to the zone. The confidence level in the case of external faults is expected to be low, which implies that the fault is not in this section of the network and, it is in adjacent cable. To test this scenario, the proposed algorithm is implemented in all PDs, shown in Fig. 4. Faults F_1–F_5 are simulated at mid-point of the cable in different sections of the microgrid. The response of the algorithm implemented in PD_{12} is studied for various faults under this section. It may be noted that the fault F_1 internal to the zone is located with the accuracy of 95% and with a confidence level of 100%. The error in the distance estimated for fault F_2 is <10% having confidence level <50%. This indicates that the fault is out of this cable section. Similarly, PD_{12} estimated the distance of fault

Table 4 Time taken by PD_{12} to estimate the fault distance and resistance

Fault distance, km	Resistance R_f, Ω					
	0.01	0.20	0.40	0.60	0.80	1.00
	Time to locate the fault distance in ms					
0.05	0.110	0.215	0.113	0.241	0.151	0.228
0.1	0.200	0.213	0.242	0.125	0.125	0.134
0.2	0.213	0.151	0.183	0.151	0.232	0.121
0.3	0.118	0.151	0.113	0.213	0.131	0.251
0.4	0.245	0.100	0.120	0.230	0.151	0.213
0.5	0.218	0.233	0.110	0.113	0.238	0.243
0.6	0.113	0.151	0.180	**4.100**	**2.300**	**2.688**
0.7	0.115	0.148	**1.200**	**2.551**	**1.551**	**2.400**
0.8	0.150	0.181	**3.413**	**1.551**	0.551	**3.688**
0.95	0.151	0.131	**2.551**	**3.413**	0.688	**3.800**

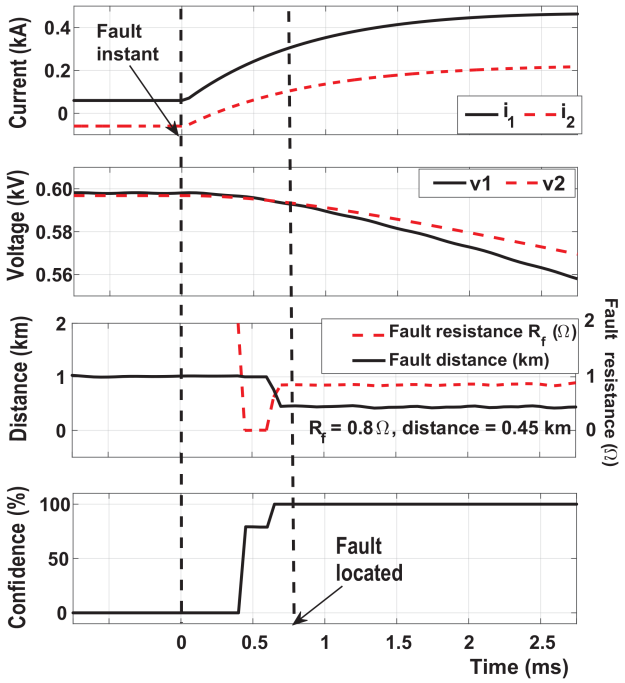

Fig. 9 *Current and voltages captured by PD_{34} and PD_{43} and fault parameters estimated by PD_{34} for pole to ground fault F_3*

F_5 with 110% error with high confidence level, as shown in Fig. 11. The distance estimation is reliable but error is >100%, which may be because the distance is estimated with the negative polarity. For faults F_3 and F_4, the estimated distance is more than the actual cable length and the confidence level is <20%. A low confidence level implies that the fault is out of the range of PD_{12} and is present in the adjacent network section, which would be detected by the corresponding PD.

4.4 Comparison with existing methods

The performance of the proposed method is also compared with the existing techniques [7, 19, 21, 22, 30, 31] suggested in the literature on the basis of extra cost required for external unit, accuracy, and time to locate the fault. A quantitative and qualitative comparison of the techniques is given in Tables 5 and 6, respectively. All the references are compared on the basis of error in fault location and time to locate the fault at distance of 1 km from the locator unit. It is observed that the performance of the proposed algorithm is comparable to those in [7, 31] in terms of cost, as these also utilise local measurements. However, Feng *et al*. [31] and the proposed method require less time to locate the fault when compared with [7], as shown in Table 6. The scheme suggested in [31] is further compared with the proposed method in terms of its accuracy for faults at different distances and resistance values.

A pole-to-pole fault F_1, shown in Fig. 4, is simulated at various distance with different fault resistances. The data captured during transients is utilised to determine the fault distance and fault resistance. The fault distance at 0–50% of cable length is estimated by PD_{12} and remaining by PD_{21}. Errors ϵ_p and ϵ_r in fault location using the proposed technique and that in Feng *et al.* [31], respectively, are shown in Table 5. It is observed that the method suggested in Feng *et al*. [31] is capable of accurately locating only those faults which are nearer to the fault locator unit. Fault at a distance of 100 m with the resistance of 10 mΩ is located with an accuracy of 99.64%. As the fault moves away from the unit and with an increase in the fault resistance, its accuracy reduces. This is due to two reasons; first, the method suggested in [31] considered the system where single source and load is utilised, and second, it assumes the passive type of load. In the case of ring architecture, where the multiple sources and loads with the power electronic converter may be present, the method in [31] may give erroneous result. This is because the fault current contributed from both the source and the loads are not modelled while estimating the fault distance in Feng *et al*. [31].

5 Conclusions

Fault location in a DC microgrid is a challenging task because of the fast isolation of the fault, and therefore less available data. Further, the presence of DC capacitors on both ends of the cable due to power electronic converters allows fault current from both

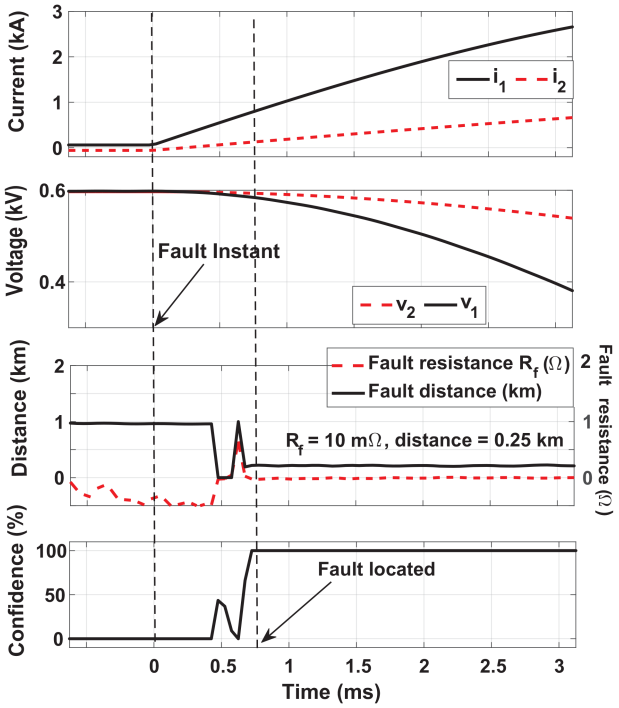

Fig. 10 *Current and voltages captured by PD_{34} and PD_{43} and fault parameters estimated by PD_{34} for fault pole to pole F_3*

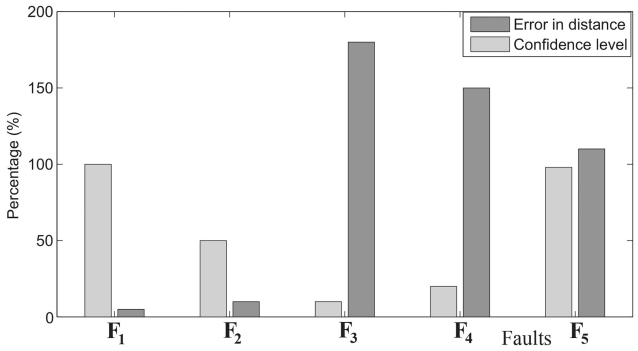

Fig. 11 *Confidence level and fault distance estimated by PD_{12} for faults F_1 to F_5*

Table 5 Percentage error in fault location by the proposed method (ϵ_p) and method in [31] (ϵ_r) in the case of pole-to-pole fault

Fault distance, km	Resistance R_f, Ω											
	Error in fault location (ε) in %											
	0.01		0.20		0.40		0.60		0.80		1.00	
	ϵ_p	ϵ_r	ϵ_p	ϵ_r	ϵ_p	ϵ_r	ϵ_p	ϵ_r	ϵ_p	ϵ_r	ϵ_p	ϵ_r
0.05	0.06	0.60	0.02	2.80	0.04	4.10	0.06	7.50	0.14	9.00	2.00	9.60
0.1	0.19	0.36	0.70	3.76	1.00	7.41	1.00	10.33	1.00	13.50	1.50	12.75
0.2	0.24	0.26	0.50	2.75	0.03	5.40	0.50	10.50	1.00	12.80	2.00	15.36
0.4	0.25	0.28	0.75	2.60	0.50	5.02	0.75	10.01	1.25	12.89	1.25	15.52
0.5	0.60	0.30	0.40	2.90	0.40	5.70	1.20	10.90	1.00	14.05	0.60	18.95
0.6	0.17	0.33	0.83	3.41	0.57	6.67	0.80	12.68	2.00	13.52	1.50	17.81
0.8	0.13	0.63	0.25	6.10	0.32	17.20	0.75	12.50	1.25	16.58	0.35	18.80
0.95	0.32	0.95	0.11	11.80	0.41	12.84	1.05	15.60	1.20	15.25	0.67	18.98

Table 6 Qualitative comparison of the existing fault location schemes

Parameters	[22]	[21]	[30]	[7]	[31]	Proposed method
required external unit?	yes	yes	no	no	no	no
communication required?	no	no	yes	no	no	no
maximum error in fault location	7%	7.8%	1.7%	12%	20%	2%
fault location time, ms	20	5	10	9.92	0.65	0.75
cost of implementation	high	high	moderate	low	low	low

the ends of the cable to contribute, unlike in conventional systems. The voltage and current transients during fault are utilised in this work to design an online fault location technique, without using any communication. A mathematical model of the faulted network is derived, which is used in the algorithm to estimate the fault location. An estimation-based method is applied on the model to accurately locate the fault and its associated fault resistance. The estimated values are further confirmed with the calculated level of confidence. The internal faults are located with error <2% and confidence level >95%. The proposed method is applicable to both pole–pole and pole-to-ground faults. Further, the algorithm has inherent property to differentiate the external and internal faults based on estimated fault distance. The proposed algorithm is independent of the microgrid topology and operating point.

6 Acknowledgment

The authors would like to thank the Department of Science and Technology (DST) Indo-US Science and Technology Forum (IUSSTF), New Delhi, India, for providing partial financial support to carry out this research work under an Indo-US project (UI-ASSIST) no. IUSSTF/EE/2017282B.

7 References

[1] Dugan, R., McDermott, T.: 'Distributed generation', *IEEE Ind. Appl. Mag.*, 2002, **8**, (2), pp. 19–25
[2] Blaabjerg, F., Teodorescu, R., Liserre, M., *et al.*: 'Overview of control and grid synchronization for distributed power generation systems', *IEEE Trans. Ind. Electron.*, 2006, **53**, (5), pp. 1398–1407
[3] Salomonsson, D., Sannino, A.: 'Low-voltage DC distribution system for commercial power systems with sensitive electronic loads', *IEEE Trans. Power Deliv.*, 2007, **22**, (3), pp. 1620–1627
[4] Starke, M., Fangxing, L., Tolbert, L.M., *et al.*: 'AC vs. DC distribution: maximum power transfer capability'. Proc. IEEE/PES Conversion Delivery Electrical Energy 21st Century, Pittsburgh, PA, USA, July 2008, pp. 1–6
[5] Starke, M., Tolbert, L., Ozpineci, B.: 'AC vs. DC distribution: a loss comparison'. Proc. IEEE/PES Transmission Distribution Conf. Exposition, Pittsburgh, PA, USA, July 2008, pp. 1–7
[6] Salomonsson, D., Soder, L., Sannino, A.: 'Protection of low-voltage DC microgrids', *IEEE Trans. Power Deliv.*, 2009, **24**, (3), pp. 1045–1053
[7] Yang, J., Fletcher, J.E., OReilly, J.: 'Short-circuit and ground fault analyses and location in VSC-based DC network cables', *IEEE Trans. Ind. Electron.*, 2012, **59**, (10), pp. 3827–3837
[8] Fletcher, S.D.A., Norman, P.J., Galloway, S.J., *et al.*: 'Optimizing the roles of unit and non-unit protection methods within DC microgrids', *IEEE Trans. Smart Grid*, 2012, **3**, (4), pp. 2079–2087
[9] Fletcher, S.D.A., Galloway, S.J., Norman, P.J., *et al.*: 'High speed differential protection for smart DC distribution system', *IEEE Trans. Smart Grid*, 2014, **5**, (5), pp. 2610–2617
[10] Meghwani, A., Srivastava, S., Chakrabarti, S.: 'A new protection scheme for DC microgrid using line current derivative'. Proc. IEEE/PES General Meeting, Denver, CO, USA, July 2015, pp. 1–5
[11] Farhadi, M., Mohammed, O.A.: 'A new protection scheme for multi-bus DC power systems using an event classification approach', *IEEE Trans. Ind. Appl.*, 2016, **52**, (4), pp. 2834–2842
[12] Mohanty, R., Pradhan, A.K.: 'Protection of smart DC microgrid with ring configuration using parameter estimation approach', *IEEE Trans. Smart Grid*, 2017, pp. 1–1, DOI: 10.1109/TSG.2017.2708743
[13] Saleh, K.A., Hooshyar, A., El-Saadany, E.F.: 'Hybrid passive-overcurrent relay for detection of faults in low-voltage DC grids', *IEEE Trans. Smart Grid*, 2017, **8**, (3), pp. 1129–1138
[14] Meghwani, A., Srivastava, S., Chakrabarti, S.: 'A non-unit protection scheme for DC microgrid based on local measurements', *IEEE Trans. Power Deliv.*, 2017, **32**, (1), pp. 172–181
[15] Duan, J., Zhang, K., Cheng, L.: 'A novel method of fault location for single-phase microgrids', *IEEE Trans. Smart Grid*, 2016, **7**, (2), pp. 915–925
[16] Aki, H. 'Demand-side resiliency and electricity continuity: experiences and lessons learned in Japan', 2017, **105**, (7), pp. 1443–1455
[17] Zadsar, M., Haghifam, M.R., Larimi, S.M.M.: 'Approach for self-healing resilient operation of active distribution network with microgrid', 2017, **11**, (18), pp. 4633–4643
[18] Butler Purry, K.L., Sarma, N.D.R.: 'Self-healing reconfiguration for restoration of naval shipboard power', *IEEE Trans. Power Syst.*, 2004, **19**, (2), pp. 754–762
[19] Park, J.D., Candelaria, J., Ma, L., *et al.*: 'DC ring-bus microgrid fault protection and identification of fault location', *IEEE Trans. Power Deliv.*, 2013, **28**, (4), pp. 2574–2584
[20] Xu, M.M., Xiao, L.Y., Wang, H.F.: 'A prony-based method of locating short-circuit fault in DC distribution system'. 2nd IET Renewable Power Generation Conf., Beijing, China, September 2013, pp. 1–4
[21] Mohanty, R., Balaji, U.S.M., Pradhan, A.K.: 'An accurate noniterative fault-location technique for low-voltage DC microgrid', *IEEE Trans. Power Deliv.*, 2016, **31**, (2), pp. 475–481
[22] Christopher, E., Sumner, M., Thomas, D., *et al.* 'Fault location in a zonal DC marine power system using active impedance estimation', *IEEE Trans. Appl. Ind.*, 2013, **49**, (2), pp. 860–865
[23] Park, J.: 'Ground fault detection and location for ungrounded DC traction power systems', *IEEE Trans. Veh. Technol.*, 2015, **64**, (12), pp. 5667–5676
[24] Kheirollahi, R., Dehghanpour, E.: 'Developing a new fault location topology for DC microgrid systems'. 7th Power Electronics, Drive Systems and Technologies Conf. (PEDSTC), Iran, 2016, pp. 1–5
[25] Jia, K., Bi, T., Liu, B., *et al.*: 'Marine power distribution system fault location using a portable injection unit', *IEEE Trans. Power Deliv.*, 2015, **30**, (2), pp. 818–826
[26] Nanayakkara, O.M.K.K., Rajapakse, D.A., Wachal, R.: 'Traveling-wave-based line fault location in star-connected multiterminal HVDC systems', *IEEE Trans. Power Deliv.*, 2012, **27**, (4), pp. 2286–2294
[27] Azizi, S., Pasand, M.S., Abedini, M., *et al.*: 'A traveling wave-based methodology for wide area fault location in multiterminal DC systems', *IEEE Trans. Power Deliv.*, 2014, **29**, (6), pp. 2552–2560
[28] Chang, C., Kumar, S., Liu, B., *et al.*: 'Real-time detection using wavelet transform and neural network of short-circuit faults within a train in DC transit systems'. *IEE Proc. Electric Power Applications*, 2001, **148**, (3), pp. 251–256
[29] Chanda, N., Yong, F.: 'Ann-based fault classification and location in MVDC ship-board power systems'. North American Power Symp., Boston, 2011, pp. 1–7
[30] Dhar, S., Patnaik, R.K., Dash, P.K.: 'Fault detection and location of photovoltaic based DC microgrid using differential protection strategy', *IEEE Trans. Smart Grid*, 2017, **99**, pp. 1–1
[31] Feng, X., Qi, L., Pan, J.: 'A novel fault location method and algorithm for DC distribution protection', *IEEE Trans. Ind. Appl.*, 2017, **53**, (3), pp. 1834–1840
[32] Xu, Z., Zhang, B., Sirisukprasert, S., *et al.*: 'Circuit breaker technologies for advanced ship power systems'. 2002 IEEE Power Engineering Society Winter Meeting, Arlington, VA, USA, May 2002, pp. 288–293
[33] Schmerda, R., Krstic, S., Wellner, E., *et al.*: 'IGCTs vs. IGBTs for circuit breakers in advanced ship electrical systems'. IEEE 2009 Electric Ship Technologies Symp. (ESTS 2009), Baltimore, MD, USA, April 2009, pp. 400–405
[34] Fletcher, S.D.A., Norman, P.J., Galloway, S.J., *et al.*: 'Determination of protection system requirements for DC unmanned aerial vehicle electrical power network for enhance capability and survivability', 2011, **1**, (4), pp. 137–147
[35] Schweppe, F.C., Masiello, R.D.: 'A tracking static state estimator', *IEEE Trans. Power Appl. Syst.*, 1971, **90**, (10), pp. 1025–1033
[36] Xu, L., Chen, D.: 'Control and operation of DC microgrid with variable generation and energy storage', *IEEE Trans. Power Deliv.*, 2011, **26**, (4), pp. 2513–2521
[37] Jover, B.: 'Choosing the right earthing system, Schneider electric: energy regulations'. Available at http://blog.schneider-electric.com/energy-regulations/2014/01/03/choosing-right-earthing-system/
[38] DC voltage transducers. Available at: http://www.europowercomponents.com
[39] DC current transducers. Available at: https://sensing.honeywell.com/